Chemical Physics Letters 661 (2016) 168–172

Contents lists available at ScienceDirect

Chemical Physics Letters

journal homepage: www.elsevier.com/locate/cplett

Research paper

Oxidation and decomposition mechanisms of air sensitive aluminum clusters at high heating rates

Jeffery B. DeLisio [a], Dennis H. Mayo [a,b], Philip M. Guerieri [a], Samantha DeCarlo [a], Ross Ives [a], Kit Bowen [c], Bryan W. Eichhorn [a], Michael R. Zachariah [a,*]

[a] Department of Chemistry and Biochemistry and Department of Chemical and Biomolecular Engineering, University of Maryland, College Park, MD 20742, USA
[b] NSWC Indian Head EOD Tech Division, Indian Head, MD 20640, USA
[c] Department of Chemistry, Johns Hopkins University, Baltimore, MD 21218, USA

ARTICLE INFO

Article history:
Received 11 April 2016
In final form 24 August 2016
Available online 26 August 2016

Keywords:
Aluminum clusters
Oxidation kinetics
Mass spectrometry

ABSTRACT

Molecular near zero oxidation state clusters of metals are of interest as fuel additives. In this work high heating rate decomposition of the Al(I) tetrameric cluster, $[AlBr(NEt_3)]_4$ (Et = C_2H_5), was studied at heating rates of up to 5×10^5 K/s using temperature-jump time-of-flight mass spectrometry (T-jump TOFMS). Gas phase Al and AlH_x species were rapidly released during decomposition of the cluster, at ~220 °C. The activation energy for decomposition was determined to be ~43 kJ/mol. Addition of an oxidizer, KIO_4, increased Al, AlO, and HBr signal intensities, showing direct oxidation of the cluster with gas phase oxygen.

1. Introduction

Metal fuels such as aluminum have been employed as additives for propellants and explosives due to their high volumetric energy densities. In a recent study, we demonstrated burn rate enhancements in a liquid hydrocarbons using a hydrocarbon soluble molecular aluminum cluster, with a near zero oxidation state, as an accelerator [1]. Specifically, there is a significant enhancement in droplet burn rate with small additions of a Al(I) tetrameric cluster, $[AlBr(NEt_3)]_4$ (Et = C_2H_5) [1]. While the combustion characteristics of aluminum cluster materials are largely unknown, the more well-studied nanosized metal particles show faster reaction kinetics and lower ignition temperatures relative to their micron-sized analogs [2]. However, with decreasing particle size, the contribution of the native oxide layer to the total mass of the particle significantly increases, thereby reducing the energy content of the particles [3,4]. In addition, the native oxide creates a barrier between the metallic fuel and any oxidizer that limits the reaction kinetics. Molecular aluminum compounds with sufficient ligand stabilization offer an intriguing alternative to nano-aluminum fuels in that oxide coatings may be circumvented giving rise to potentially new combustion mechanisms and enhanced oxidation kinetics [5,6]. However, until fundamental properties of these clusters are studied, such as their compatibility with oxidizers in a composite, their utility as a fuel remains unclear.

Because the oxidation mechanisms of ligated Al clusters are unknown, their combustion characteristics are difficult to predict. For example, if combustion of the ligand shell precedes the combustion of the Al core, then any enhancement in combustion rate relative to Al NPs may be overshadowed. Simulations by Hooper and coworkers [7–9] suggest that oxidation of aluminum precedes that of the ligand shell in $Cp*_4Al_4$ clusters but mechanistic experimental data on these processes are necessary to further develop these models. To study aluminum cluster oxidation, we require the ability to investigate air-sensitive compounds via thermally-activated chemistry on a time scale and with heating rates nominally associated with an ignition event encountered in combustion, as previous studies have demonstrated that reaction pathways can vary greatly between slow and fast heating [10–12]. In prior work, we have employed a temperature-jump time-of-flight mass spectrometer (T-jump TOFMS) to probe decomposition of nitrocellulose and RDX [13], the reaction mechanisms of nanothermite systems [14–17], and activation energies for oxygen release from metal oxides [18].

In this study, we build on our previous work on T-jump TOFMS with the incorporation of an air sensitive sample holder (ASSH) capable of heating samples at rates of up to 5×10^5 K/s [13]. The ASSH enables loading of air sensitive samples in a glove box and transfer to the TOFMS without ambient exposure. In this paper we study the high heating rate decomposition of $[AlBr(NEt_3)]_4$ in an oxygen-free environment as well as its oxidation with bismuth

* Corresponding author.
E-mail address: mrz@umd.edu (M.R. Zachariah).

http://dx.doi.org/10.1016/j.cplett.2016.08.065
0009-2614/

oxide (Bi_2O_3) and potassium periodate (KIO_4). These results also demonstrate that a molecular aluminum fuel ($AlBr(NEt_3)]_4$,)can be in immediate physical contact with a strong oxidizer (KIO_4 or Bi_2O_3) and remain stable under an inert atmosphere.

2. Experimental

2.1. Materials

The tetrameric Al(I) cluster $[AlBr(NEt_3)]_4$ was synthesized from an $AlBr{\bullet}NEt_3$ starting material produced in a Schnöckel-type metal halide co-condensation reactor (MHCR) [19–21]. A rendering of the cluster's crystal structure is shown in Fig. 1.

Bismuth oxide (Bi_2O_3) nanopowder was purchased from Sigma Aldrich. Potassium periodate (KIO_4) nanoparticles were prepared by dissolving KIO_4 (Sigma Aldrich) in distilled water and then using a previously described aerosol based spray drying procedure [22]. Hexane was dried over sodium benzophenone ketyl and stored over activated 3Å molecular sieves.

2.2. Air sensitive sample holder

A custom-built air-sensitive sample holder (ASSH) was used with a previously described temperature-jump time-of-flight mass spectrometer (T-jump TOFMS) [13]. The ASSH uses a ~25 μm thick aluminum foil membrane to prevent oxygen exposure of the sample while transporting the holder to the TOFMS. The membrane is sealed using a gasket compressed by a threaded cap at the end of a stainless steel housing that surrounds the T-jump probe. A 3D printed collar (designed in SolidWorks and printed using a Stratasys Objet30 Pro) was fixed to the electrical feedthrough of the T-jump probe. This collar punctures the aluminum foil membrane when inserted into the TOFMS.

2.3. Sample preparation

Samples were prepared in a glovebox with 2 mg of combined solids suspended in 1 mL of dry hexane. Mixed samples containing the $[AlBr(NEt_3)]_4$ cluster and Bi_2O_3 or KIO_4 (1:3 cluster to oxidizer ratio by mass) were sonicated for 10 min in a sealed, oxygen-free vial. Samples were loaded as a suspension in hexanes via autopipette onto 76 μm platinum (Pt) wires held by the ASSH within the glove box. The ASSH sample holder was then capped under inert atmosphere, removed from the glovebox, and transferred to the TOFMS.

2.4. Sample analysis

During standard operation, the roughing chamber of the TOFMS is pumped and purged with UHP nitrogen (N_2) gas prior to mounting the ASSH. N_2 was chosen over argon due its lower background signal intensity. A positive pressure of N_2 is maintained in the roughing chamber during mounting of the ASSH, after which the aluminum foil membrane is punctured and the roughing chamber evacuated to ~0.5 torr. Once the roughing chamber is evacuated, the gate valve to the main chamber of the TOFMS is opened and the sample inserted. When the system is under vacuum, the platinum wires are resistively heated within the TOFMS (sampling rate = 10 kHz) with time resolved wire temperatures calculated using the Callendar-Van Dusen equation. A 600 MHz digital oscilloscope was used for data acquisition. To perform activation energy analysis, wire heating rates were varied between 1×10^5 and 5×10^5 K/s by increasing or decreasing the pulse width and/or driving voltage of the heating circuit. With the exception of the experiments used in determining the activation energy, a heating rate of $\sim 4 \times 10^5$ K/s was employed. All mass spectra signal intensities were normalized to the maximum signal intensity of $m/z = 86$ (the predominant fragment observed from electron impact ionization of NEt_3) unless otherwise noted.

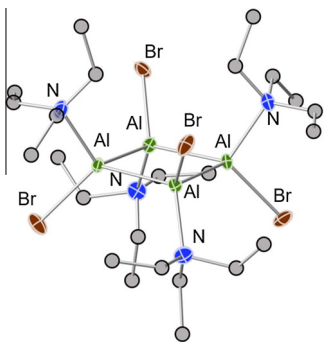

Fig. 1. X-ray crystal structure of $[AlBr(NEt_3)]_4$ [21]. Thermal ellipsoids drawn at 50% probability level. Unlabeled grey spheres represent carbon; hydrogen atoms omitted for clarity.

3. Results and discussion

3.1. Thermal decomposition of $[AlBr(NEt_3)]_4$ during rapid heating

Analysis of the decomposition of $[AlBr(NEt_3)]_4$ was performed on both oxidized and unoxidized samples. Analysis of the data was complicated by the fact that the mass of aluminum ion ($m/z = 27$) also corresponds to the mass of any ethyl fragments generated by the direct decomposition of triethylamine (NEt_3). Unfortunately, the analogous trimethylamine and tripropylamine complexes of AlBr are not known, which precludes the resolution of the mass degeneracy by chemical substitution. When ionized using electron impact ionization, pure NEt_3 has multiple mass envelopes between the m/z values of 27 and 101 with the highest relative signal intensity corresponding to the $m/z = 86$ fragment [23]. Since the peak at m/z 86 is solely a result of NEt_3 decomposition, we employed it as an internal reference standard to normalize the signal intensities. Fig. 2 shows the spectra at the time of the maximum absolute $m/z = 86$ signal intensity for the unoxidized $[AlBr(NEt_3)]_4$ introduced via ASSH (Fig. 2a), and after exposure to the ambient atmosphere for ~3 h (Fig. 2b).

We find that peaks corresponding to m/z values of 27, 28, 29, and 30 have much higher signal intensities prior to oxidation (Fig. 2a). When exposed to oxygen, the NEt_3 remains intact but the Al in the cluster oxidizes, resulting in decreased signal intensities in the 27–30 mass envelope seen in Fig. 2b. The spectrum of the oxidized cluster in Fig. 2b also shows an increased H_2O signal intensity and the presence of AlO and HBr species (discussion below). To highlight the differences in the decomposition of unoxidized and oxidized $[AlBr(NEt_3)]_4$, a difference plot was generated using the normalized spectrum at the time of maximum $m/z = 86$ signal intensity for the oxidized sample and the unoxidized sample as seen in Fig. 2c. The difference spectrum removes all peaks associated with NEt_3 decomposition and highlights the Al containing species in the anaerobic sample and the H_2O, AlO, and HBr in the oxidized signal. The increased normalized signal intensity of the $m/z = 27$ peak of the unoxidized sample affirms that reactive aluminum is present in the system and is being generated during decomposition of the cluster. During rapid decomposition under anaerobic conditions, the Al(I) tetrameric cluster will presumably react with hydrogen-containing fragments from the NEt_3. Thus, we conclude that signals in the 27–30 m/z range in the difference spectrum (Fig. 2c) correspond to Al, AlH, AlH_2, and AlH_3.

The observed Br and HBr in the oxidized sample is a result of hydrolysis of $[AlBr(NEt_3)]_4$ [4]. In the presence of air, the aluminum

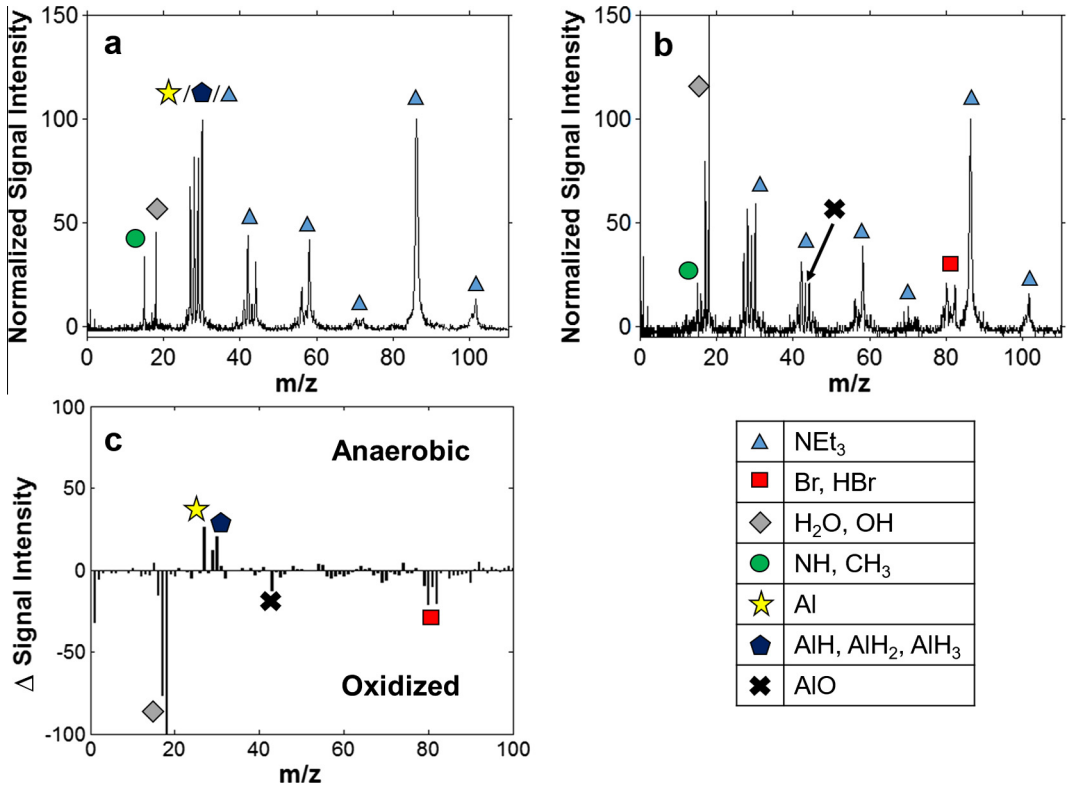

Fig. 2. Normalized MS at time of maximum $m/z = 86$ signal intensity (0.8 ms, ~330 °C) for the anaerobic (a) and oxidized (b) Al(I) tetrameric cluster heated at ~4×10^5 K/s and normalized difference spectrum (c) of anaerobic – oxidized.

in the complex reacts with ambient oxygen and water to form HBr and AlO containing species (e.g. Al_2O_3, Al(O)OH, etc.). The HBr will react with NEt_3 to give the non-volitle $HNEt_3Br$ salt that decomposes back HBr and NEt_3 when heated. The formation of this salt prevents NEt_3 from evaporating/decomposing during air oxidation, allowing the use of NEt_3 fragments as an internal standard for our study. Previous temperature-programmed reaction (TPR) experiments have detected generation of HBr when heating $[AlBr(NEt_3)]_4$ in the presence of water. This observation is consistent with the T-jump TOFMS results for the oxidized and KIO_4-containing samples (see Fig. S2 and discussion below) [1].

3.2. Reactions of $[AlBr(NEt_3)]_4$ mixed with oxidizers

The next phase of this study proceeded with the introduction of oxidizers to the $[AlBr(NEt_3)]_4$ suspensions. Two different oxygen-containing nanoparticles, Bi_2O_3 and KIO_4, were physically mixed with the cluster prior to deposition onto the Pt filament. Bi_2O_3 is known to have low ignition temperatures in aluminum-based nanothermite compositions and has been shown to initiate reaction through the condensed phase [24]; KIO_4 also exhibits low ignition temperatures with aluminum and is known to release gas phase oxygen at a low temperatures prior to ignition [22]. These two oxidizers should provide insight into the reactivity of $[AlBr(NEt_3)]_4$ in the both solid- and gas-phase.

The samples containing Bi_2O_3 did not alter the decomposition of the $[AlBr(NEt_3)]_4$ cluster, with no increase in $m/z = 43$ (AlO) signal intensity, implying little discernable contribution from this oxidizer (see Fig. S1). As previously stated, Bi_2O_3 is believed to oxidize Al nanoparticles by condensed phase transport of oxygen, which implies that the Al(I) tetrameric cluster decomposes before oxygen becomes mobile in the oxidizer. This is further supported by temporal analysis (Section 3.3), which shows that the tetramer decomposes several hundred degrees lower than when oxygen becomes mobile, and thus gas-phase decomposition products will have escaped before they have an opportunity to be oxidized. Previous studies have shown that at high heating rates, condensed-phase reaction with Bi_2O_3 begins at ~627 °C for carbon and Al-based thermites [24]. The Al(I) tetrameric cluster decomposes and Al is gasified well below ~627 °C, preventing the Bi_2O_3 from oxidizing the Al (decomposition temperatures discussed in Section 3.3). Further, these results demonstrate that $[AlBr(NEt_3)]_4$ is able to be in immediate physical contact and sonicated with a strong condensed phase oxidizer (Bi_2O_3) without reaction occurring during the sample preparation for this experiment.

The mass spectrum for the rapidly heated $[AlBr(NEt_3)]_4/KIO_4$ mixture (Tet-KIO_4) in Fig. S2 shows the detection of AlO and HBr species indicating that oxidation of the $[AlBr(NEt_3)]_4$ has occurred during heating. An increased amount of H_2O is observed that is due to the oxidation of the cluster's ligands in addition to any residual H_2O within the KIO_4 that is released during decomposition. A decrease in the $m/z = 15$, corresponding to NH/CH_3, is also apparent when KIO_4 is present. The effects of gas phase oxygen generated by the KIO_4 on the reaction mechanism of the rapidly heated $[AlBr{\cdot}NEt_3]_4$ is further described in the temporal analysis section.

As shown with the pure tetramer samples, the species overlap between Al and AlH and NEt_3 fragmentation is still an issue when analyzing samples mixed with an oxidizer, therefore the data were treated in the same fashion as previously described. Table 1 lists normalized integrated signal intensities for $m/z = 27$ and 30 of the unoxidized Al(I) tetrameric cluster and the mixture with KIO_4.

The pure and mixed samples both show identical integrated signal intensities for the $m/z = 27$ peak during rapid heating. The integrated signal intensity for the $m/z = 30$ peak decreases when KIO_4 is added to the system, therefore the ratio of the $m/z = 27$ to $m/z = 30$ is higher for the mixture. The $m/z = 30$ signal intensity is

Table 1
Normalized $m/z = 27$ and $m/z = 30$ integrated signal intensity values during rapid heating of the unoxidized Al(I) tetrameric cluster (Tet) and Al(I) tetrameric cluster mixed with KIO_4 (Tet+KIO_4).

Sample	Integrated signal intensity $m/z = 27$	Integrated signal intensity $m/z = 30$	Ratio 27:30
Tet	72	91	0.79
Tet + KIO_4	72	62	1.16

partially attributed to the formation of AlH_3 under anaerobic conditions. The integrated signal intensity of $m/z = 43$ was doubled when KIO_4 was added due to the aforementioned formation of AlO. In the presence of KIO_4, the more favorable AlO species is formed and the amount of AlH_x is diminished.

3.3. Temporal speciation

The previous TPR experiments on $[AlBr(NEt_3)]_4$ employed a much slower heating rate (10 °C/min) than the T-jump TOFMS system, and the onset of cluster decomposition was observed at ~50 °C [1]. The TPR experiments, however, did not examine species with an m/z less than 50, therefore no conclusions on gas phase aluminum release can be drawn. As shown by the spectra in Fig. 2a, the Al(I) tetrameric cluster releases gas phase Al resulting in the increased $m/z = 27$ signal intensity in comparison to the oxidized sample in Fig. 2b. For the oxidized and unoxidized $[AlBr(NEt_3)]_4$, all detected species appear in the time resolved spectra concurrently pointing towards a single step decomposition of the cluster. In Fig. 3, we show temporal results from T-jump TOFMS for the $m/z = 27$ species for neat $[AlBr(NEt_3)]_4$ and Tet-KIO_4. Fig. 3 also shows that at a heating rate of $\sim 4 \times 10^5$ K/s, decomposition of the anaerobic neat tetramer occurs at ~220 °C. The Al contribution to the $m/z = 27$ signal over time for unoxidized $[AlBr(NEt_3)]_4$ is shown in Fig. S3.

The addition of KIO_4 resulted in a delayed, yet higher intensity $m/z = 27$. As shown in Table 1 above, both the pure and mixed samples had the same integrated signal intensities for the $m/z = 27$ peak. The addition of KIO_4 delays the detection of gas phase Al in the MS, but the amount detected is unchanged. We propose that some of the gas phase Al released from cluster decomposition reacts with the surface of the KIO_4 particles during cluster decomposition. The sharp high intensity $m/z = 27$ peak in Fig. 3 occurs concurrently with KIO_4 decomposition. A similar delay is observed with Bi_2O_3 as well, where Bi_2O_3 has no oxidizing effect (see Fig. S4). The gas phase Al on the surface of the Bi_2O_3 desorbs before the oxygen in the Bi_2O_3 is able to react, therefore the $m/z = 27$ peak is delayed, but does not have a higher intensity as seen in the KIO_4 mixture.

Samples containing KIO_4 appear to alter the decomposition of $[AlBr(NEt_3)]_4$, as observed in Fig. 4, which shows the temporal behavior of $m/z = 43$, which can be primarily be attributed to AlO. The m/z of 43, for the pure tetramer, corresponds to a minor fragment from NEt_3 ionization. Thus the observed enhanced m/z 43 with KIO_4 addition can be attributed to oxidation of Al to AlO by gas phase oxygen from KIO_4.

This attribution is further confirmed by the temporal O_2 release seen in Fig. 5 between neat KIO_4 and KIO_4 mixed with $[AlBr(NEt_3)]_4$ tetramer (Tet-KIO_4). These signal intensities were normalized to $m/z = 39$, corresponding to potassium being released from the decomposition of KIO_4.

Previous work has shown KIO_4 to undergo a two stage decomposition, which is consistent with the results shown in Fig. 5 [22]. The onset temperatures for decomposition of the KIO_4 are identical for both neat KIO_4 and Tet-KIO_4, but a significant decrease in the first stage of oxygen release is observed for Tet-KIO_4. This decrease can be attributed to the oxygen being consumed by the reaction with Al from the $[AlBr(NEt_3)]_4$ cluster. It is also important to note that the peak O_2 signal intensity occurs at the same time/temperature as the peak $m/z = 43$ signal intensity of the Tet-KIO_4 in Fig. 4, further supporting the proposed mechanism of Al from the cluster combining with gas phase O_2 generated by the KIO_4 to form AlO.

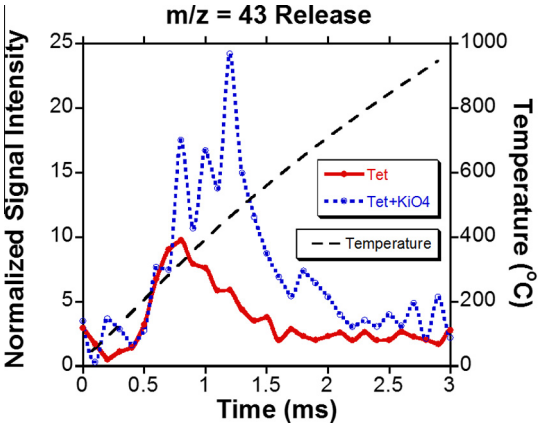

Fig. 4. Species over time plot of $m/z = 43$ for the pure Al(I) tetrameric cluster (Tet) and the Al(I) tetrameric cluster mixed with KIO_4 (Tet-KIO_4).

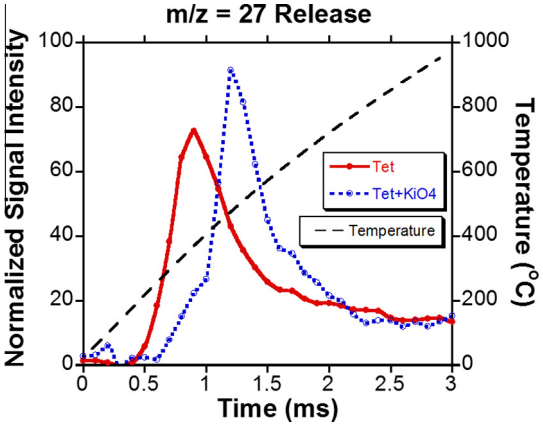

Fig. 3. $m/z = 27$ release over time for the pure Al(I) tetrameric cluster (Tet) and the Al(I) tetrameric cluster mixed with KIO_4 (Tet-KIO_4).

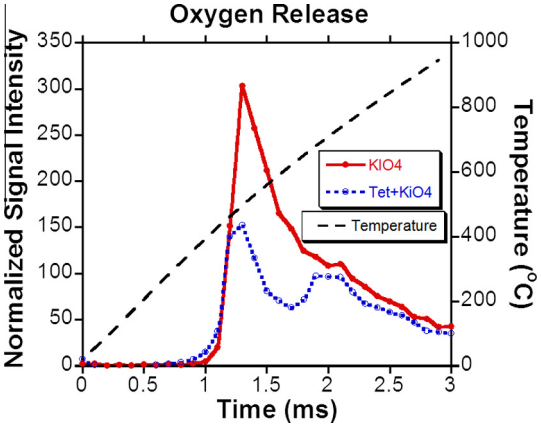

Fig. 5. Oxygen release over time for pure KIO_4 and the Al(I) tetrameric cluster mixed with KIO_4 (Tet-KIO_4).

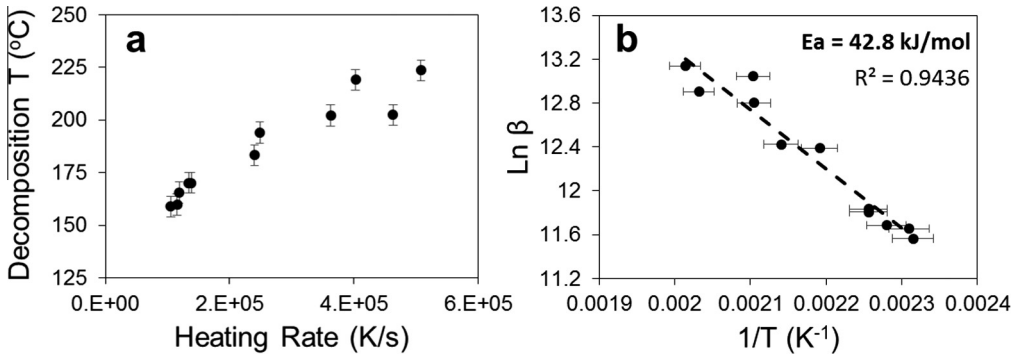

Fig. 6. Decomposition temperature (first appearance of $m/z = 86$) vs heating rate (a) and Arrhenius plot (b) of rapidly heated unoxidized Al(I) tetrameric cluster.

3.4. Activation energy for Al(I) tetrameric cluster decomposition

The activation energy for the decomposition of the Al(I) tetrameric cluster was obtained using the Flynn-Wall-Ozawa isoconversional method, similar to previous work done by Jian et al. using T-jump TOFMS [18]. The decomposition temperature was defined as the temperature of the Pt filament when the highest intensity NEt_3 fragment, $m/z = 86$, was first detected by the TOFMS. Fig. 6a shows the decomposition temperature as a function of heating rate, which as expected, increases with increasing heating rate. Fig. 6b shows the resulting Arrhenius plot of heating rate, β, vs. the inverse of the decomposition temperature and yields an activation energy for decomposition of 42.8 kJ/mol for $[AlBr(NEt_3)]_4$.

While the activation energy appears to be small, low activation energies appear to be consistently observed in a variety of systems under high heating rate conditions. For example, the activation energy for oxygen release from CuO nanoparticles at high heating rates was found to be at least 2–3 times lower than that under heating rates consistent with normal TGA measurements [18].

3.5. Al(I) tetrameric cluster reaction mechanism summary

At high heating rates, decomposition of the Al(I) tetrameric cluster, $[AlBr(NEt_3)]_4$, occurs between ~160 and ~220 °C as shown in Fig. 6a. Decomposition releases NEt_3 fragments and gas phase Al, which under anaerobic conditions forms AlH_x species. When heated after exposure to ambient oxygen, an increase in HBr is observed. No significant evidence of a condensed phase oxidation of the cluster was observed as demonstrated by the lack of AlO species when Bi_2O_3 was mixed with $[AlBr(NEt_3)]_4$. In contrast, use of a low temperature gas –generator (KIO_4) showed the presence of AlO as a reaction product along with a decrease in AlH_x species. As gas phase oxygen is neccessary for oxidation of this particular Al(I) cluster, future Al cluster/oxidizer systems may be tailored to have simultaneous Al and O_2 release to maximize Al oxidation. This work shows that $[AlBr(NEt_3)]_4$ can be intimately mixed and sonicated in a suspension with strong oxidizers (Bi_2O_3 and KIO_4) without room temperature reactions occurring, demonstrating the potential of aluminum cluster materials as ingredients in energetic formulations.

Acknowledgments

The authors gratefully acknowledge support from the Office of Naval Research (Program Director Clifford Bedford) under ONR Grant# N00014-15-1-2681, AFOSR (MURI) and DTRA for support.

Appendix A. Supplementary data

Supplementary data associated with this article can be found, in the online version, at http://dx.doi.org/10.1016/j.cplett.2016.08.065.

References

[1] P.M. Guerieri, S. DeCarlo, B. Eichhorn, T. Connell, R.A. Yetter, X. Tang, Z. Hicks, K.H. Bowen, M.R. Zachariah, J. Phys. Chem. A 119 (2015) 11084.
[2] E.L. Dreizin, Prog. Energy Combust. Sci. 35 (2009) 141.
[3] R.A. Yetter, G.A. Risha, S.F. Son, Proc. Combust. Inst. 32 (2009) 1819.
[4] C.E. Aumann, G.L. Skofronick, J.A. Martin, J. Vac. Sci. Technol., B 13 (1995) 1178.
[5] J.M. Lightstone, C. Stoltz, R.M. Wilson, J. Horn, J. Hooper, D. Mayo, B. Eichhorn, K. Bowen, M.G. White, 7th Biennial Conference of the American-Physical-Society-Topical-Group on Shock Compression of Condensed Matter, Amer Inst Physics, Chicago, IL, 2011.
[6] K.S. Williams, J.P. Hooper, J. Phys. Chem. A 115 (2011) 14100.
[7] S. Alnemrat, J.P. Hooper, 18th Joint Int Conf of the APS Topical-Grp on Shock Compress of Condensed Matter / 24th Int Conf of the Int-Assoc-for-the-Advancement-of-High-Pressure-Sci-and-Technol, Iop Publishing Ltd, Seattle, WA, 2013.
[8] S. Alnemrat, J.P. Hooper, J. Chem. Phys. 141 (2014) 7.
[9] S. Alnemrat, J.P. Hooper, J. Chem. Phys. 140 (2014) 7.
[10] M. Schoenitz, S. Umbrajkar, E.L. Dreizin, J. Propul. Power 23 (2007) 683.
[11] S.M. Umbrajkar, M. Schoenitz, E.L. Dreizin, Thermochim. Acta 451 (2006) 34.
[12] T.B. Brill, M.C. Beckstead, J.E. Flanagan, M.C. Lin, T.A. Litzinger, R.H.W. Waesche, C.A. Wight, J. Propul. Power 18 (2002) 824.
[13] L. Zhou, N. Piekiel, S. Chowdhury, M.R. Zachariah, Rapid Commun. Mass Spectrom. 23 (2009) 194.
[14] L. Zhou, N. Piekiel, S. Chowdhury, M.R. Zachariah, J. Phys. Chem. C 114 (2010) 14269.
[15] G. Jian, L. Zhou, N.W. Piekiel, M.R. Zachariah, Chem. Phys. Processes Combust. (2011) 126.
[16] G. Jian, N.W. Piekiel, M.R. Zachariah, J. Phys. Chem. C 116 (2012) 26881.
[17] G. Jian, S. Chowdhury, K. Sullivan, M.R. Zachariah, Combust. Flame 160 (2013) 432.
[18] G. Jian, L. Zhou, N.W. Piekiel, M.R. Zachariah, ChemPhysChem 15 (2014) 1666.
[19] P.L. Timms, Acc. Chem. Res. 6 (1973) 118.
[20] M. Tacke, H. Schnoeckel, Inorg. Chem. 28 (1989) 2895.
[21] M. Mocker, C. Robl, H. Schnoeckel, Angew. Chem. 106 (1994) 1860.
[22] G. Jian, J. Feng, R.J. Jacob, G.C. Egan, M.R. Zachariah, Angew. Chem., Int. Ed. 52 (2013) 9743.
[23] S.E. Stein, Mass Spectra, in: P.J. Linstrom, W.G. Mallard (Eds.), NIST Chemistry WebBook, NIST Standard Reference Database Number 69, National Institute of Standards and Technology, Gaithersburg MD, 20899, <http://webbook.nist.gov>, (retrieved March 28, 2016).
[24] N.W. Piekiel, L. Zhou, K.T. Sullivan, S. Chowdhury, G.C. Egan, M.R. Zachariah, Combust. Sci. Technol. 186 (2014) 1209.